Phase difference effect on collective locomotion of two tandem autopropelled flapping foils

Xingjian Lin,[1,2] Jie Wu,[3,1,2,*] Tongwei Zhang,[1,2] and Liming Yang[4]
[1]*Department of Aerodynamics, Nanjing University of Aeronautics and Astronautics, Yudao Street 29, Nanjing, Jiangsu 210016, China*
[2]*Key Laboratory of Unsteady Aerodynamics and Flow Control, Ministry of Industry and Information Technology, Nanjing University of Aeronautics and Astronautics, Yudao Street 29, Nanjing, Jiangsu 210016, China*
[3]*State Key Laboratory of Mechanics and Control of Mechanical Structures, Nanjing University of Aeronautics and Astronautics, Yudao Street 29, Nanjing, Jiangsu 210016, China*
[4]*Department of Mechanical Engineering, National University of Singapore, 10 Kent Ridge Crescent, Singapore 119260*

(Received 24 January 2019; published 17 May 2019)

The effect of phase difference on the collective locomotion of two tandem flapping foils is numerically studied in this paper. The numerical results indicate that the collective locomotion is greatly affected by the phase difference. Two distinct collective modes are observed, i.e., the fast mode and the slow mode. The fast mode is only observed in part of the range of the phase difference (ϕ), i.e., $\phi = 0.0-0.1\pi$ and $1.5\pi-1.9\pi$ with appropriate initial distance, and the slow mode appears in the range of $\phi = 0.3\pi-1.4\pi$. Meanwhile, the follower of the two foils has hydrodynamic benefit in both fast and slow modes, and it can obtain the highest efficiency in the fast mode at $\phi = 1.6\pi$. However, the leader can only achieve hydrodynamic benefit in the fast mode, and the highest efficiency occurs at $\phi = 0.1\pi$. In addition, the stable distance between two foils in the slow mode can be quantized with the phase difference. Furthermore, the fluid-structure interactions between two foils are also analyzed. Two distinct vortex interactions are observed in the fast mode, i.e., merging interaction and broken interaction, which, respectively, result in the highest propulsive efficiency for the follower and the leader. In the merging interaction, the leading edge vortex of the leader is captured by the follower, which results in the weak trailing edge vortex of the leader but a strong trailing edge vortex of the follower. In the broken interaction, the leading edge vortex of the follower sheds into the wake together with the trailing edge vortex of the leader, and induces the trailing edge vortex of the follower to be broken into two parts. Which kind of vortex interaction occurs depends on the phase difference. The results obtained here may provide some light on understanding the coordinated behavior of biological collectives.

DOI: 10.1103/PhysRevFluids.4.054101

I. INTRODUCTION

The collective locomotion of multiple moving bodies has recently become a transdisciplinary research focus. It is not only ubiquitous in biological systems [1,2], but also may have implications for the optimization of artificial machines, such as artificial flying or swimming robots and energy harvester devices [3,4]. As typical examples of biological systems with collective motions, fish

*wuj@nuaa.edu.cn

school and bird flocks have been interesting to biologists, physicists, and engineers for several decades [5–10]. Several benefits have been verified for such collective behaviors, such as foraging and antipredator behavior [1]. From the fluid mechanics perspective, it is also considered that the hydrodynamic benefit can be obtained from collective behaviors [7–13]. Moreover, Lighthill once pointed out that the hydrodynamic force alone is enough for the emergence of collective locomotion [14]. However, the hydrodynamic mechanism of such collective behaviors is still controversial so far [15,16]. One of the primary challenges for understanding animal collective behaviors is that the collective flow-structure interactions are very complicated, since there is complex coupling between flows and moving bodies.

Attempting to understand the collective behaviors of fish school and bird flocks, a number of experimental and numerical studies have been carried out [17–21]. In order to simplify the question and consider the biological morphology, an animal collective can be simplified as two flapping foils or hydrofoils in several arrangements [22,23]. For the tandem formation, it has been indicated that the performance of the downstream body is affected by the wake of the upstream body [17,24,25], since the oncoming flow and the effective angle of attack of the follower are changed by the vortices shed from the leader [26,27]. The thrust enhancement can be achieved by the follower when it slaloms between the vortices [25,27], while the thrust of the leader can be enhanced when the spacing is small [17], because the wake splitting occurs at the leading edge of the follower [24]. In addition, the performance augmentation of two flapping foils has also been observed for the other arrangements [19,21]. However, in these previous studies, the individuals were fixed in the flow, which only has the response of the flow to the bodies' movement with the lack of the response of the bodies' locomotion to the flow. Thus, such simplified models still have restrictions on the investigations of collective behaviors.

In order to further investigate the hydrodynamic mechanism in the coordinated behaviors in animal collectives, the self-propelled model has been developed recently [28,29]. Zhu *et al.* have shown that orderly formations can be formed by two tandem self-propelled flapping foils through the flow-mediated interactions, in which the trajectory of the follower was also locked onto the vortex cores shed from the leader [30]. Furthermore, the collective behaviors of multiple self-propelled flapping foils have recently been observed [31]. On the other hand, the collective locomotion of two flapping foils was also investigated experimentally [32]. Ramananarivo *et al.* have shown that the hydrodynamic force can prompt and retain the coordinated locomotion, and the separation distance between individuals can be quantized with the wavelength traced out by the leader [33]. However, for the possible purpose of simplifying the problem, only the in-phase motion was discussed in these studies. But in nature, it is hard to find the uniform in-phase motions in animal collectives; instead the phase difference is more likely to be observed. The collective behaviors of two autopropelled flapping foils with phase difference have not been sufficiently investigated; learning more about the effect of the phase difference on the collective behaviors of animal collectives is the motivation of the current work.

In this paper, the effect of the phase difference on the collective behaviors of two self-propelled flapping foils is numerically studied in detail. As shown in Fig. 1, two self-propelled flapping foils are arranged in tandem formation initially, and the autopropulsion of each foil is driven by a harmonic motion. The simulations are carried out via an immersed boundary method based on a simplified circular function–based gas kinetic scheme [34,35]. The numerical results indicate that the collective locomotion is significantly affected by phase difference. Two collective modes are identified according to the propulsive velocity, i.e., the fast mode and the slow mode. Which kind of mode occurs depends on the phase difference. In addition, the collective fluid-structure interactions are analyzed for collective locomotion. Two distinct vortex interactions are observed in the fast mode, i.e., merging interaction and broken interaction. Moreover, the stable separating distance between two foils in the slow mode has been quantized with phase difference.

The remainder of this paper is organized as follows. The problem description and methodology are presented in Sec. II. The simulation results are addressed in detail with discussion in Sec. III. Finally, some conclusions are drawn in Sec. IV.

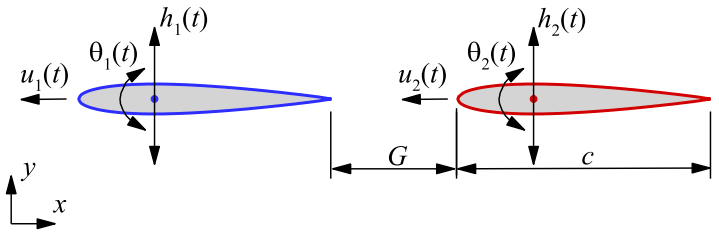

FIG. 1. Sketch view of the simulation model, i.e., two flapping foils in tandem arrangement. $h(t)$ and $\theta(t)$, respectively, represent the heaving and pitching motions; $u(t)$ is the propelled velocity; subscripts 1 and 2, respectively, represent the variables of leading and trailing foils. G is the horizontal separation gap between two foils; c is the chord length. The pivot location of the pitching motion is fixed at $c/3$ for both foils.

II. PROBLEM DESCRIPTION AND METHODOLOGY

A. Problem description

In this paper, the two-dimensional NACA 0012 airfoil with the chord length of c is used as the profile of the autopropelled flapping foil. As shown in Fig. 1, two flapping foils are arranged in tandem formation with the initial longitudinal spacing G_0. Both foils are driven by harmonic motions as follows:

$$h_1(t) = A_1 \sin(2\pi f_1 t), \quad \theta_1(t) = \alpha_1 \cos(2\pi f_1 t), \tag{1a}$$

$$h_2(t) = A_2 \sin(2\pi f_2 t + \phi), \quad \theta_2(t) = \alpha_2 \cos(2\pi f_2 t + \phi), \tag{1b}$$

where $h(t)$ and $\theta(t)$, respectively, are the instantaneous heaving and pitching motions of the flapping foils, f is the flapping frequency, A is the heaving amplitude, α is the pitching amplitude, and the subscripts 1 and 2, respectively, represent the variables of leading and trailing foils. ϕ is the phase difference between two flapping foils. The pivot location of the pitching motion is fixed at $c/3$ for both foils.

The propulsion of each foil is controlled by the Newton's second law, which can be described as

$$m\frac{d^2\mathbf{X}}{dt^2} = \mathbf{F}, \tag{2}$$

where $\mathbf{X} = (X, Y)$ is the dimensionless position vector of the foil; $\mathbf{F}$ is the hydrodynamic force applied on the foil surface, which results from the hydrodynamic interactions. $m = (\rho_s s)/(\rho c^2)$ is the dimensionless mass of the foil which is determined by the density ratio $\bar{\rho} = \rho_s/\rho$, where ρ_s and ρ are the densities of foil and fluid, respectively, and s represents the area of the foil. Both foils are set as free and can self-propel in the horizontal direction (x direction) due to the force generated from the hydrodynamic interactions, but there is no motion in the vertical direction. In this paper, the positive thrust and propelled direction are defined along the negative x direction. The instantaneous dimensionless propelled velocity of each foil can be calculated as

$$u(t) = \frac{dX}{dt}. \tag{3}$$

Meanwhile, the cycle-averaged power consumption of each foil can be calculated as

$$P_m = \frac{1}{T}\int_t^{t+T} \left[\left|F_y \frac{dh(t)}{dt}\right| + \left|M\frac{d\theta(t)}{dt}\right|\right] dt, \tag{4}$$

where T is the flapping period; F_y and M are the vertical force and torque applied on the foil surface, respectively. Thus, the propulsive efficiency is defined as

$$\eta = \frac{E_k}{P_m T}, \tag{5}$$

where $E_k = \frac{1}{T}\int_t^{t+T} \frac{1}{2} m u^2 dt$ is the output power, i.e., the kinetic energy of each foil.

In addition, other parameters, i.e., thrust coefficient and power coefficient, are calculated as follows:

$$C_T = \frac{-2F_x}{\rho U^2 c}, \quad C_p = \frac{2P_m}{\rho U^3 c}, \tag{6}$$

where F_x is the horizontal force; $U = 2\pi fA$ is the characteristic velocity.

Moreover, since the self-propelled velocity of the flapping foil fluctuates in the steady swimming state [36], the cycle-averaged distance and velocity are also calculated for analysis, i.e.,

$$\bar{G} = \frac{1}{T}\int_t^{t+T} G(t)dt, \quad \bar{u} = \frac{1}{T}\int_t^{t+T} u(t)dt, \tag{7}$$

where $G(t)$ is the instantaneous horizontal separation gap between two foils.

B. Numerical method and validation

The two-dimensional viscous flow over the flapping foils is simulated in the current work, and the governing equations can be written as follows:

$$\frac{\partial \rho}{\partial t} + \nabla \cdot (\rho \mathbf{u}) = 0, \tag{8}$$

$$\frac{\partial \rho \mathbf{u}}{\partial t} + \nabla \cdot (\rho \mathbf{u}\mathbf{u}^T + p\mathbf{I}) = \nu \nabla \cdot [\nabla(\rho \mathbf{u}) + \nabla(\rho \mathbf{u})^T], \tag{9}$$

where $\mathbf{u}$ is the flow velocity vector, p is the pressure, ν is the kinematic viscosity of flow, and $\mathbf{I}$ is the unit tensor. The Reynolds number is defined as $\mathrm{Re} = Uc/\nu$ in the current work. A simplified circular function–based gas kinetic method [34,35] is adopted to solve Eqs. (8) and (9), and a velocity correction–based immersed boundary method [37] is used to deal with the fluid-structure interactions between the flapping foils and the surrounding flow. For more details about the numerical method used in this study, one can refer to our previous work [34,35,37].

Although the numerical method and the corresponding code have been validated with other numerical results in our previous work [34,35], the experimental validation is carried out in the current work. The previous experimental work of Wang [38] is selected for the current numerical validation, in which the stationary fluid condition is the same as that in the current work. The kinematics of the airfoil is controlled as follows:

$$[x(t), y(t)] = \frac{A_0}{2c}\cos(2\pi ft)(\cos\beta, \sin\beta), \tag{10a}$$

$$\alpha(t) = \alpha_0 + \alpha_m \sin(2\pi ft), \tag{10b}$$

where $[x(t), y(t)]$ are the coordinates of the center of the airfoil; $\alpha(t)$ and α_0 are the instantaneous and initial angles of attack of the airfoil, respectively. A_0/c is the dimensionless flapping amplitude, β is the inclined angle of the stroke plane with respect to the horizontal direction, and α_m is the rotating amplitude. The Reynolds number for this problem is defined as $\mathrm{Re}_0 = A_0\pi fc/\nu$. The parameters are set as $\mathrm{Re}_0 = 75$, $\beta = 0$, $A_0/c = 2.8$, $\alpha_0 = \pi/2$, and $\alpha_m = \pi/4$. The validation simulation is carried out in a computational domain of $25c \times 20c$ with the domain of $4c \times 4c$ around the foil, in which the mesh size is $\Delta h = 0.01c$. The Dirichlet boundary condition is applied on the boundaries of computational domain, and the no-slip boundary condition is applied on the foil surface. The lift and drag coefficients are shown in Fig. 2. It is clear that the present results agree well with the experimental and numerical results in Ref. [38]. Consequently, the adopted method is suitable for the current investigation.

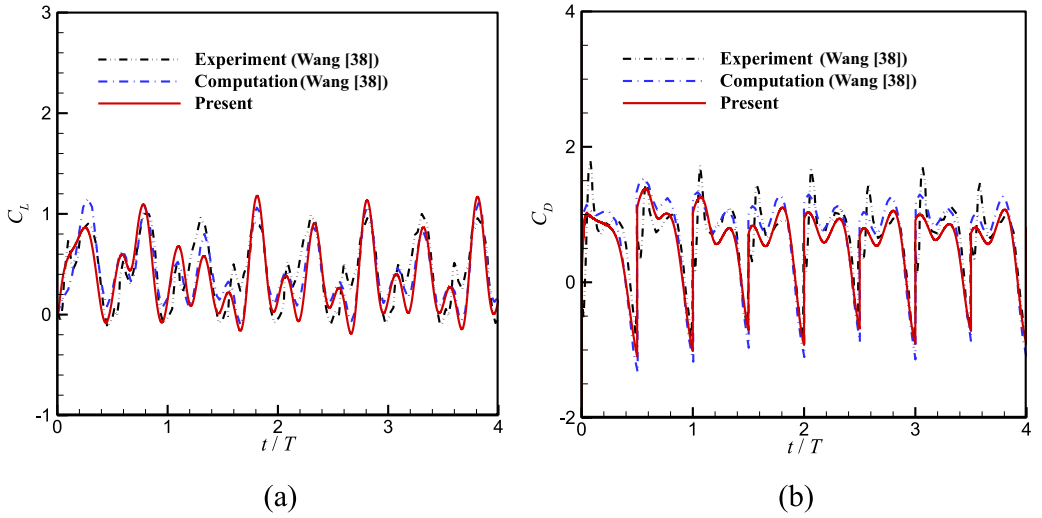

FIG. 2. Comparisons of (a) lift and (b) drag coefficients with previous results.

III. RESULTS AND DISCUSSION

In the current work, the coordinated locomotion of two tandem flapping foils is studied. The controlled parameters used in this work are listed in Table I. The size of the rectangular computational domain is $80c \times 20c$, in which the size of fine and uniform domain is $70c \times 10c$ with $\Delta h = 0.01c$. The foil surface is represented by 204 Lagrangian points with uniform distribution. The no-slip boundary condition is applied on the foil surface, and the Dirichlet boundary condition is applied on the boundaries of the computational domain. In order to make sure that the results obtained here are independent of the mesh spacing, a sensitivity test has been accomplished. As shown in Fig. 3, it can be seen that the propulsive velocity obtained from the mesh of $\Delta h = 0.01c$ is very close to that obtained from the mesh of $\Delta h = 0.005c$. To strike a balance between computational expense and accuracy that related to mesh, a grid of $\Delta h = 0.01c$ is chosen for the current simulations.

A. States of collective locomotion

The propulsive velocity is the key parameter to quantify the performance of two tandem flapping foils. In the current simulations, both foils of most cases can obtain the same cycle-averaged velocity after several flapping periods. Consequently, the orderly formation with certain separation distance is achieved by the tandem foils. However, the exception also appears in three cases, i.e.,

TABLE I. Values of the controlled parameters used in the current simulations.

Parameters	Values
Re	200
$\bar{\rho}$	10
A_1, A_2	$0.4c$
f_1, f_2	0.3
θ_1, θ_2	$\pi/9$
G_0/c	0.1, 0.25, 0.5, 0.75, 1.0, 1.25, 1.5, 2.0, 3.0
ϕ	$0\pi - 1.9\pi\,(\Delta = 0.1\pi)$

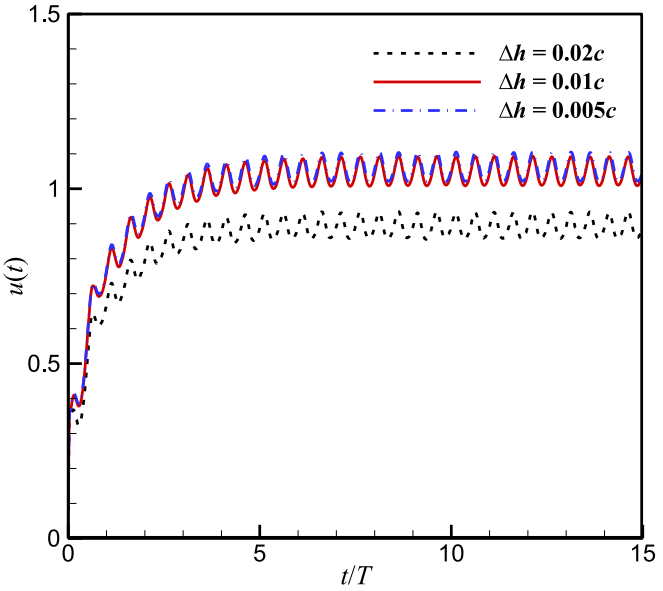

FIG. 3. Time histories of the propulsive velocity of a single flapping foil obtained from different mesh spacing. The flapping parameters are the same as that used in the current work, i.e., $f = 0.3$, A=0.4, $\theta = \pi/9$, $\bar{\rho} = 10$, and Re $= 200$.

($\phi = 0.2\pi$, $G_0 = 0.1c, 0.25c$) and ϕ(=0.3π, $G_0 = 0.1c$). It is observed that the collision between two foils occurs in such cases; namely, the distance becomes zero which results in stopping of the simulation immediately. In this section, the propulsive velocity is selected for analysis firstly, and then two distinct modes are classified, i.e., the fast mode and the slow mode. In the fast mode, a significant velocity augmentation can be observed, which is larger than 5% as compared with the single foil, and in the slow mode, the propulsive velocity of two tandem foils is close to that of the isolated foil, in which the velocity variation is less than 5%.

Figure 4 shows the ratio of cycle-averaged velocity of the tandem foils to that of the isolated foil. The fast mode is observed in the cases located in the gray region in Fig. 4(b), and the slow mode is observed in the rest of the cases, except three cross symbols which represent the collision that occurred in these cases. It is clear that the fast mode is determined by both phase difference and initial distance. In the current work, the fast mode is observed in the cases of ($\phi = 1.5\pi - 1.9\pi$, $G_0 = 0.1c - c$), ($\phi = 0\pi - 0.1\pi$, $G_0 = 0.1c - 0.5c$), ($\phi = 1.5\pi$, $G_0 = 1.25c$), and ($\phi = 0\pi$, $G_0 = 0.75c$). In the fast mode, the propulsive velocity augmentation is affected by the phase difference. For instance, in the region of $\phi = 1.5\pi - 1.9\pi$, the averaged velocity of tandem foils in the fast mode is increased with the rise of phase difference. The stable averaged separation distance ($\bar{G}$) is illustrated in Fig. 5. It is clear that, in the fast mode, $\bar{G}$ is very small (approximately $0.1c$–$0.3c$). However, in the slow mode, $\bar{G}$ is significantly larger than that in the fast mode. Moreover, it is found that the variation of $\bar{G}$ with G_0 is piecewise for a given ϕ, and it is constant during each subregion of G_0. For a fixed G_0, $\bar{G}$ can generally vary with ϕ during each subregion of ϕ, and there is a jump of $\bar{G}$ between different subregions which is determined by the G_0 and ϕ. In addition, $\bar{G}$ also can be quantized and it will be discussed in a later section.

The significant observation from Figs. 4 and 5 is that the fast mode only occurs in the cases with appropriate phase difference, not in all phase differences. It means that the fast mode is also affected by the phase difference, not only affected by the initial separation distance that has been observed in previous work [30,31,33]. Moreover, the capacity of the tandem foil system to maintain the fast mode is also affected by the phase difference. The tandem foil system with $\phi = 1.5\pi - 1.9\pi$

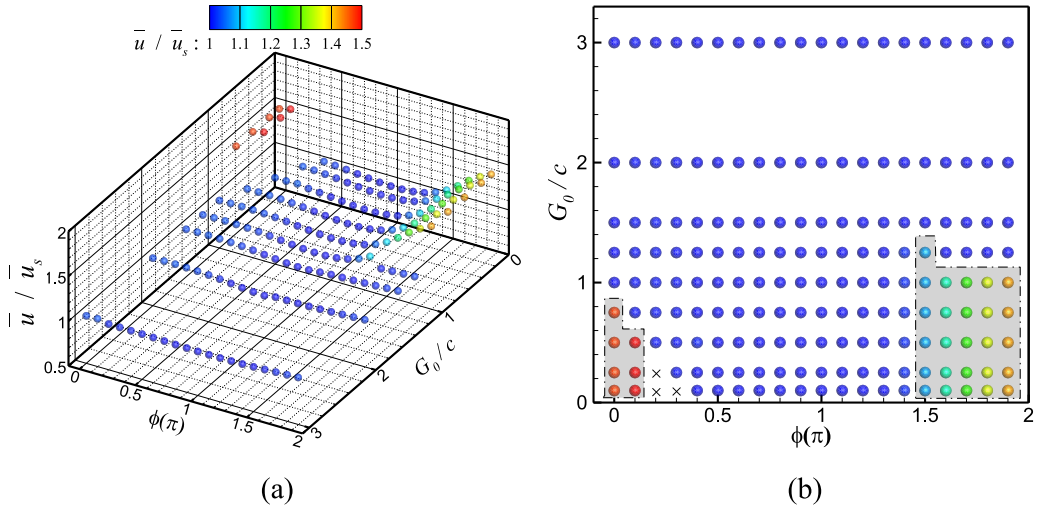

FIG. 4. (a) The ratio of the stable propulsive velocities of tandem foils and single foil, and (b) is the planform of (a). The cross symbols in (b) represent the cases in which the collision happens (the same below). The gray region represents the parameter space in which the fast mode is observed (the same below).

has high capacity to maintain the fast mode, as compared with the in-phase tandem foil system. On the other hand, the maximum velocity augmentation is not achieved by the in-phase system. In the current work, the maximum velocity augmentation is achieved at $\phi = 0.1\pi$ and $G_0 = 0.1c{-}0.5c$, in which the averaged dimensionless velocity is approximately 1.58, which is more than a 50% increment as compared with the single foil case ($(\bar{u}_s = 1.05)$.

In addition, the power consumption and propulsive efficiency of each foil are also analyzed and compared to those of the isolated foil, as shown in Figs. 6 and 7. It can be seen that the leading foil needs to consume more power in the fast mode, as shown in Fig. 6(a). However, its propulsive efficiency is significantly increased as compared with the single foil. The maximum augmentation

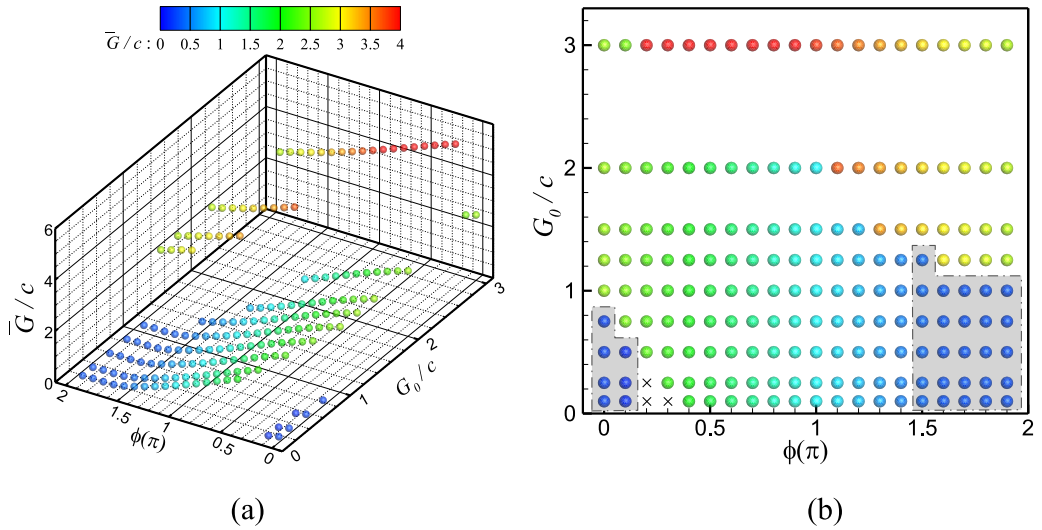

FIG. 5. (a) The stable distance between two foils in the current simulations, and (b) is the planform of (a).

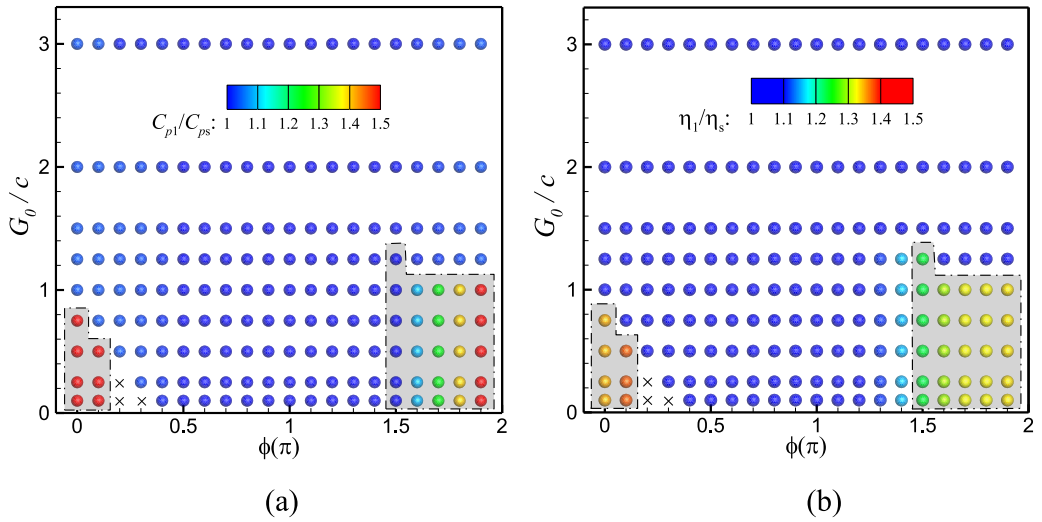

FIG. 6. The ratio of the (a) power coefficients and (b) propulsive efficiencies between the leading foil in tandem formation and the single foil.

of efficiency is achieved when $\phi = 0.1\pi$ and $G_0 = 0.1c{-}0.5c$, which is approximately 38.9%, with an increment of about 37%. In the slow mode, the power consumption and efficiency of the leading foil are close to those of the single foil, which is the same as the situation of its propulsive velocity. It means that the leader of the two tandem foil system only has hydrodynamic benefit in the fast mode.

As for the follower in the tandem formation, it is interesting that less power consumption as compared with the single foil is observed in the fast mode when $\phi = 1.5\pi{-}1.7\pi$, although high propulsive velocity is generated. However, more power consumption is also required for the follower in the fast mode region when $\phi = 0.0{-}0.1\pi$ and $1.8{-}1.9\pi$, as shown in Fig. 7(a). Similar to the leader in the fast mode, the follower also has high propulsive efficiency, as shown in Fig. 7(b), but

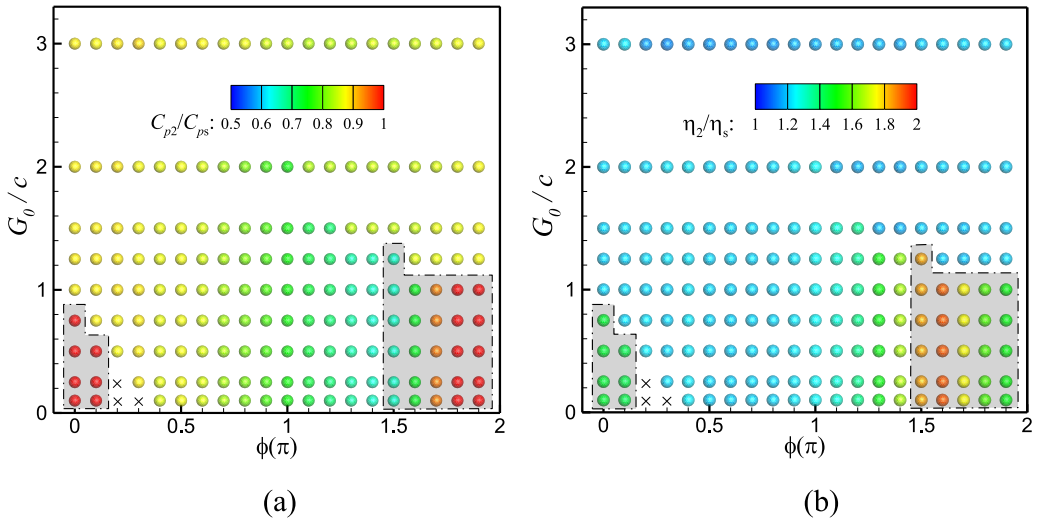

FIG. 7. The ratio of the (a) power coefficients and (b) propulsive efficiencies between the trailing foil in tandem formation and the single foil.

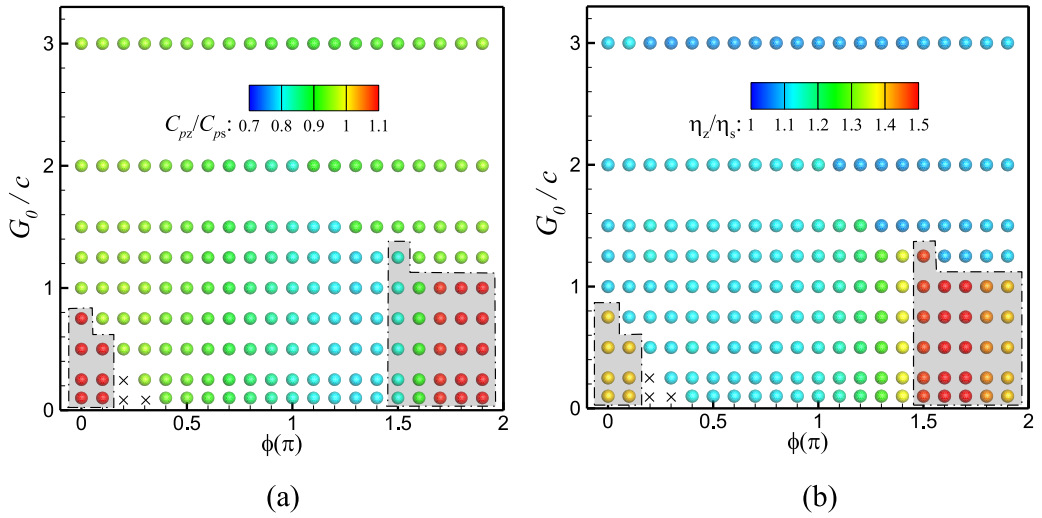

FIG. 8. The ratio of the (a) power coefficients and (b) propulsive efficiencies between the whole tandem system and the single foil.

the highest propulsive efficiency is achieved at $\phi = 1.6\pi$ and $G_0 = 0.1c-c$, instead of $\phi = 0.1\pi$ and $G_0 = 0.1c-0.5c$, in which the highest velocity is obtained. The highest propulsive efficiency of the follower is approximately 54.3%, an increment of about 90% as compared with the single foil. In addition, the follower also consumes less power in the slow mode as compared with the isolated one, although the same averaged velocity is achieved. Consequently, the high propulsive efficiency is obtained by the follower in the slow mode. However, the augmentation of the efficiency of the follower in the slow mode is smaller than that in the fast mode. It means that the follower has hydrodynamic benefit in both fast and slow modes, especially in the fast mode.

The power consumption and efficiency of the whole two tandem foil system are provided in Fig. 8. It can be seen from the figure that the whole system nearly consumes less power as compared with the single foil, except in the fast mode with $\phi = 0.0\pi-0.1\pi$ and 1.7π–1.9π. In addition, the whole system always produces high propulsive efficiency in both fast and slow modes, especially in the fast mode. The maximum efficiency of the whole system is achieved in the fast mode at $\phi = 1.6\pi$ and $G_0 = 0.1c-c$, which is about 43.8%, increased by approximately 55% as compared with the isolated one. However, it should be pointed out that, besides the initial distance and the phase difference, the collective locomotion behavior of two tandem foils is also affected by the density ratio $\bar{\rho}$. For the fixed ϕ and G_0, the collective locomotion state may change from the fast mode to the slow mode as $\bar{\rho}$ increases and vice versa. This is because the lighter foils are more sensitive to fluid-structure interaction than the heavier foils [39]. In addition, in the fast or slow mode, the cycle-averaged propulsive velocity and power consumption of tandem foils are independent of $\bar{\rho}$. Therefore, the effect of $\bar{\rho}$ on the collective locomotion of two tandem foils is not discussed in detail in the current work.

B. Performance of fast mode

In the fast mode, for a fixed phase difference, the final stable distance is not dependent on the initial distance, as shown in Fig. 9(a), for example ($\phi = 1.6\pi$). However, for a fixed initial distance, it is found that the final stable distance is related to the phase difference, as shown in Fig. 9(b), for example ($G_0 = 0.5c$). This is caused by the different fluid-structure interactions between two foils. Two distinct fluid-structure interactions are observed in the fast mode, i.e., merging interaction and broken interaction. The merging interaction appears in the cases of $\phi = 1.5\pi-1.7\pi$, and the broken

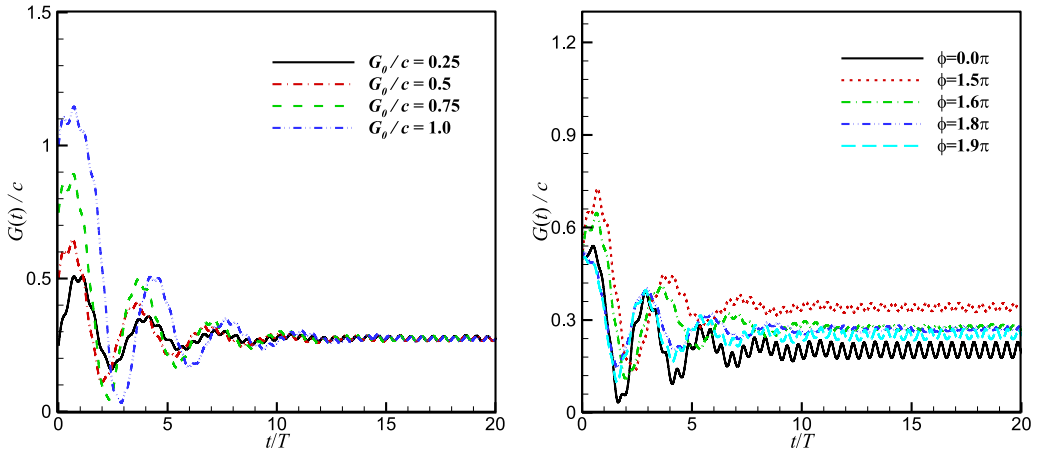

(a) (b)

FIG. 9. The time histories of the distance between two tandem flapping foils with (a) $\phi = 1.6\pi$ and (b) $G_0 = 0.5c$.

interaction is observed in the cases of $\phi = 0.0\pi - 0.1\pi$ and $1.8\pi - 1.9\pi$. Considering the propulsive efficiency reported above, it seems that the merging interaction is beneficial for the follower to get a high efficiency, while the broken interaction is good for the leader to achieve a high efficiency. In order to quantitatively describe such two different fluid-structure interactions, two typical cases with $\phi = 1.6\pi$, $G_0 = c$ and $\phi = 0.1\pi$, $G_0 = 0.5c$, respectively, are selected as examples of merging and broken interactions in this section.

When the merging interaction occurs, the leading edge vortex (LEV) of the leader is captured by the follower, and merges with the LEV of the follower. Figure 10 shows the process of merging vortex interaction for the case of $\phi = 1.6\pi$ and $G_0 = c$. It can be seen that the LEVs of both foils ($\mathrm{LEV1_{F1}}$ and $\mathrm{LEV1_{F2}}$), respectively, develop at the beginning of one cycle, as shown in Fig. 10(a).

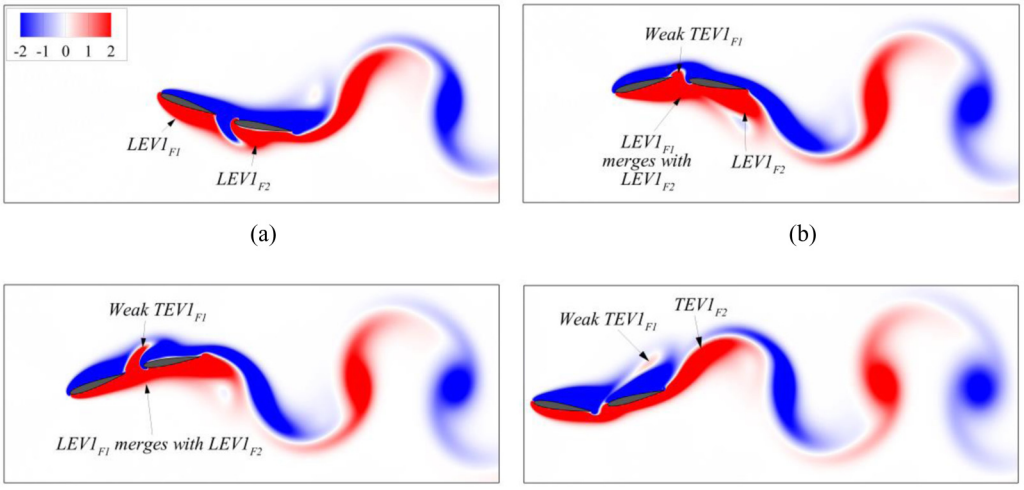

(a) (b)

(c) (d)

FIG. 10. Instantaneous vorticity at (a) $t = 0.05T$, (b) $0.4T$, (c) $0.55T$, and (d) $0.85T$ for the case of $\phi = 1.6\pi$ and $G_0 = c$.

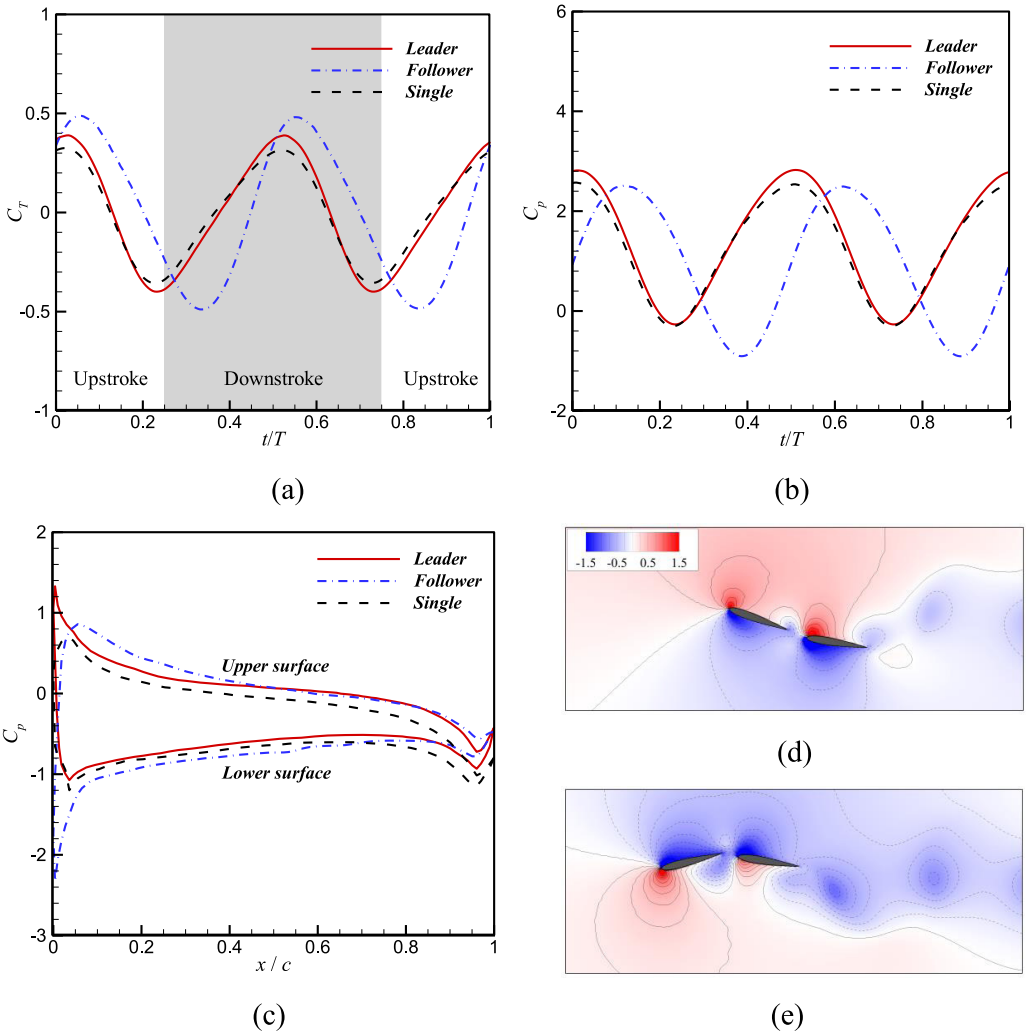

FIG. 11. The time histories of (a) thrust coefficients and (b) power coefficients of tandem foils and single foil. (c) Instantaneous pressure coefficient distribution along the surfaces of the foils at $t/T = 0.05$. Instantaneous pressure coefficient contours of tandem foils at (d) $t/T = 0.05$ and (e) 0.4 for the case of $\phi = 1.6\pi$ and $G_0 = c$.

Then, LEVs of both foils shed from the leading edges and transport along the foil surfaces. However, as shown in Fig. 10(b), $\mathrm{LEV1_{F1}}$ is captured by the follower and starts to merge with $\mathrm{LEV1_{F2}}$. This process is different from the isolated foil whose LEV is captured by itself and merges with its trailing edge vortex (TEV). Thus, only weak TEV is generated by the leader when the merging interaction occurs, as shown in Fig. 10(c). In addition, such weak $\mathrm{TEV1_{F1}}$ dissipates quickly later, as shown in Fig. 10(d). Consequently, there are only two opposite vortices shed into the wake from the trailing edge of the trailing foil in one cycle, which results in the normal reversed von Kármán vortex street in the wake. Since both $\mathrm{LEV1_{F1}}$ and $\mathrm{LEV1_{F2}}$ are captured by the follower, the strong TEV can be generated by the follower as compared with the single one, such as the $\mathrm{TEV1_{F2}}$ as shown in Fig. 10(d). Consequently, two tandem foils swim like a whole large flapping foil.

Figure 11(a) shows the time histories of thrust coefficients of tandem foils and single foil for the case of $\phi = 1.6\pi$ and $G_0 = c$. It is clear that the thrust peaks of the leader and the follower are

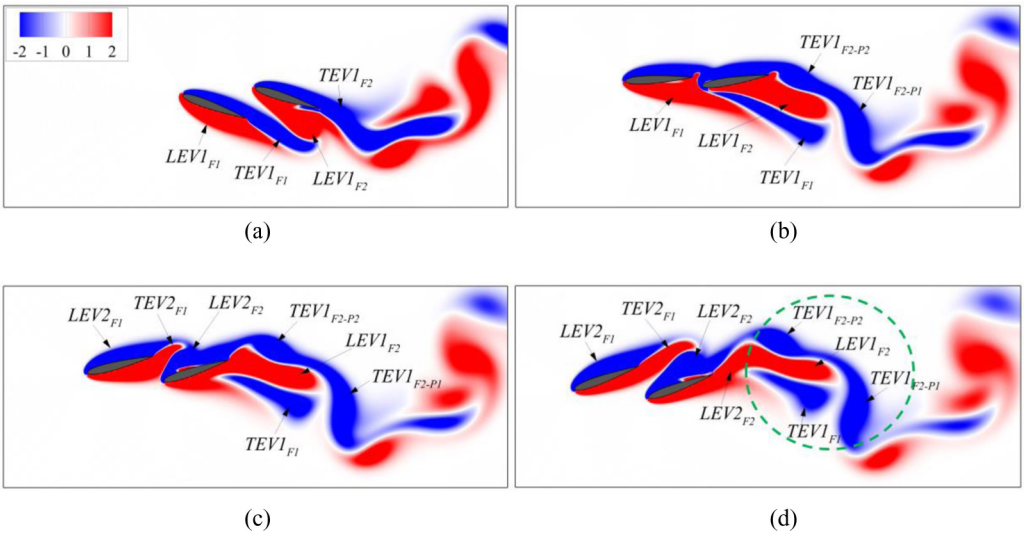

FIG. 12. Instantaneous vorticity at (a) $t = 0.05T$, (b) $0.3T$, (c) $0.4T$, and (d) $0.5T$ for the case of $\phi = 0.1\pi$ and $G_0 = 0.5c$.

higher than that of the single foil. There are two reasons for the higher thrust peak of the follower. Firstly, there exists a negative pressure region near the leading edge of the follower, as in Figs. 11(c) and 11(d), which has a suction effect on the follower. This negative pressure region is produced by the trailing edge vortex of the leader. Secondly, it can be seen from Fig. 11(c) that the pressure difference between upper and lower surfaces of the follower is larger than that of the isolated foil. Such phenomenon also can be found for the leading foil. Consequently, the leader generates a high thrust peak as compared with the isolated one.

Although the cycle-averaged thrust is zero in the steady self-propulsion, the propulsive velocity can be quantitatively analyzed by the averaged positive thrust in the upstroke or downstroke of one period. If more averaged positive thrust in one stroke is generated by the flapping foil, then the higher velocity can be generated. For instance, as shown in Fig. 11(a), in one stroke for the case of $\phi = 1.6\pi$ and $G_0 = c$, the averaged positive thrust coefficients of leader and follower, respectively, are $\bar{C}_T = 0.12$ and 0.15, which are larger than that of the single one, $\bar{C}_T = 0.10$. Since the follower has to overcome the jet flow of the leader, the large thrust is required for the follower as compared with the leader. The time histories of the power coefficients of tandem foils and single foil are illustrated in Fig. 11(b). It is clear that the follower performs the energy extraction at $t = 0.4T$ and $0.9T$. Since the LEV of the leader is captured by the follower at those moments (such as $\mathrm{LEV1_{F1}}$ is captured at $t = 0.4T$), the LEV induces the flow streams toward the follower, which results in the positive pressure on the lower surface of the follower, as shown in Fig. 11(e). Thus, a positive lift is applied to the follower at this moment, whose direction is the same as the flapping direction. Consequently, the follower can extract the energy from the flow.

In the broken interaction, the TEV of the leading foil sheds into the wake together with the LEV of the trailing foil, which causes the TEV of the trailing foil to be broken into two parts. For instance, Fig. 12 shows the instantaneous vorticity at four different instants in the half period for the case of $\phi = 0.1\pi$ and $G_0 = 0.5c$. It can be seen that $\mathrm{TEV1_{F1}}$ sheds into the region nearby the $\mathrm{LEV1_{F2}}$ at the beginning of one cycle, which induces the synchronous shedding of $\mathrm{LEV1_{F2}}$, as shown in Fig. 12(a). When $\mathrm{LEV1_{F2}}$ is close to $\mathrm{TEV1_{F2}}$, the $\mathrm{TEV1_{F2}}$ is broken into two parts, i.e., $\mathrm{TEV1_{F2-}}_{p1}$ and $\mathrm{TEV1_{F2-}}_{p2}$ as shown in Fig. 12(b). Moreover, $\mathrm{TEV1_{F1}}$ is cut off by the trailing foil when its flapping direction is changed, since both foils are too close to each other. Then, the new TEV of the leading foil ($\mathrm{TEV2_{F1}}$) is formed along the other surface, which also induces the shedding of

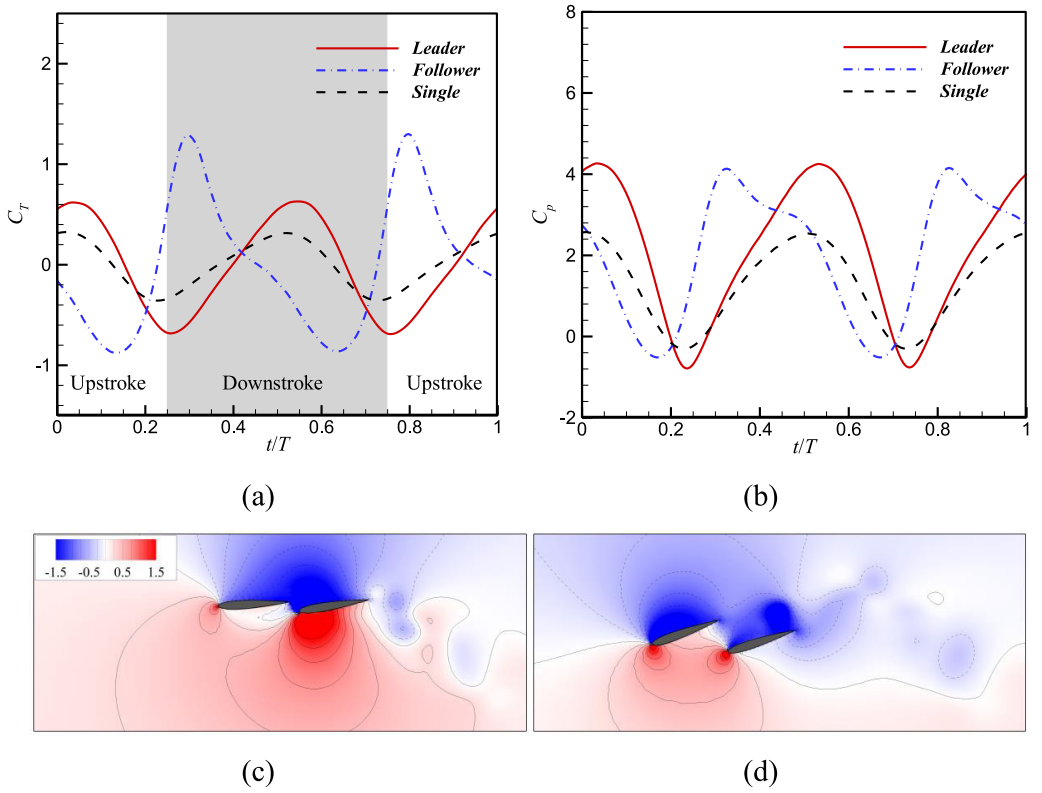

FIG. 13. The time histories of (a) thrust coefficients and (b) power coefficients of tandem foils ($\phi = 0.1\pi$ and $G_0 = 0.5c$) and a single foil. Instantaneous pressure coefficient contours of tandem foils at (c) $t/T = 0.3$ and (d) 0.55 for the case of $\phi = 0.1\pi$ and $G_0 = 0.5c$.

the new LEV of the trailing foil ($\mathrm{LEV2_{F2}}$), as shown in Fig. 12(c). Consequently, the similar vortex interaction occurs in the other half period, as shown in Fig. 12(d). It should be noted that there are four vortices shed into the wake in the half period when the broken interaction happens, as shown in the green dashed circular region of Fig. 12(d), which results in the complex vortex structure in the wake.

Figure 13(a) shows the time histories of thrust coefficients of tandem foils and a single foil for the case of $\phi = 0.1\pi$ and $G_0 = 0.5c$. The averaged positive thrust coefficients of leader and follower, respectively, are $\bar{C}_T = 0.19$ and 0.25. As expected, the averaged positive thrust coefficients of tandem foils in one stroke are larger than that of the single foil. However, compared with the single one, more power is also required for the tandem foils as shown in Fig. 13(b). Moreover, the thrust augmentation of the follower mainly occurs nearby $t = 0.3T$ and $0.8T$.

As shown in Fig. 13(c), there exists a significant positive high pressure region nearby the lower surface of the follower as compared with the leader, which results in the thrust augmentation. The reason may be that the shedding $\mathrm{LEV1_{F2}}$ induces the flow streams toward the lower surface of the follower, as shown in Fig. 12(b). In addition, the thrust augmentation of the leader mainly occurs near $t = 0.05T$ and $0.55T$. Since both foils are close to each other, the positive pressure on the leading edge of the follower also increases the positive pressure on the lower surface of the leader, as shown in Fig. 13(d).

In order to further quantitatively describe the fast mode and the two vortex interactions, the vertical gap between the trailing edge of the leading foil and the leading edge of the trailing foil is calculated. It can be defined as $D_V = y1 - y2$, where $y1$ and $y2$, respectively, represent the

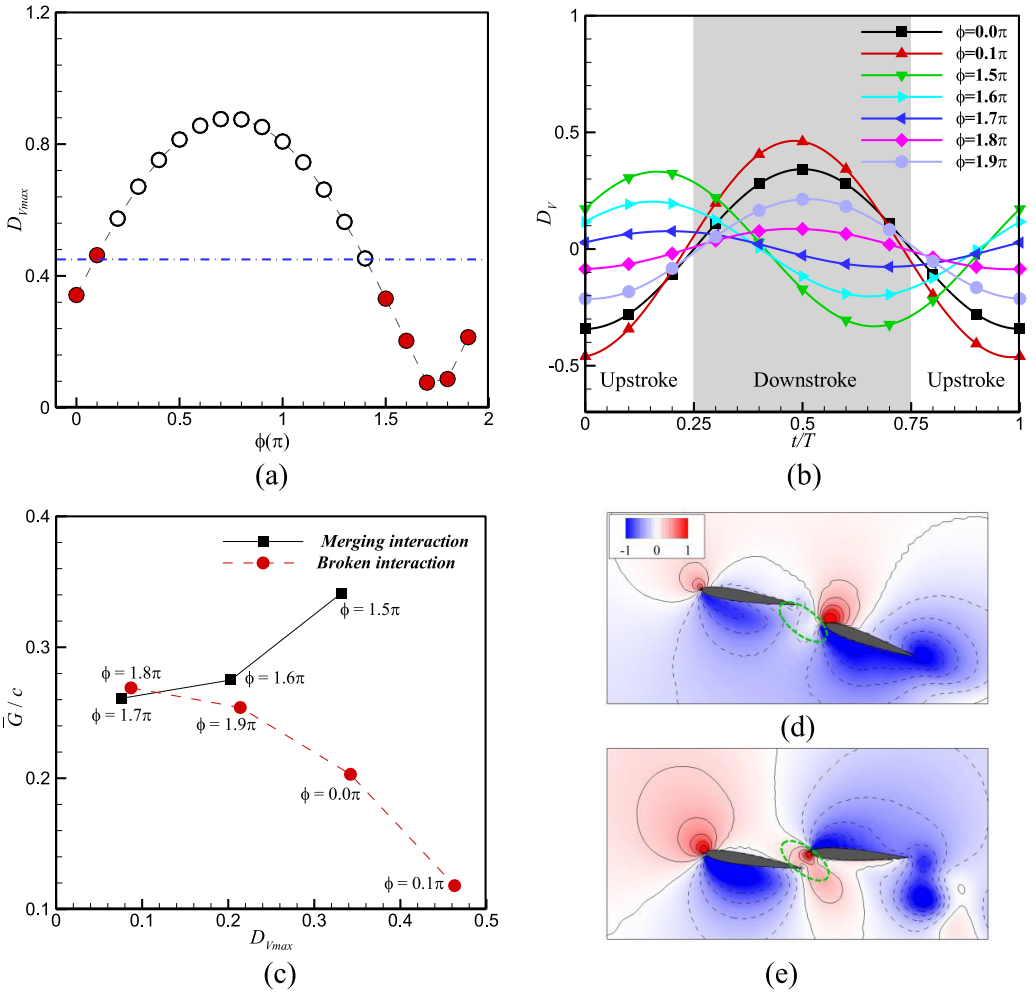

FIG. 14. (a) The maximum value and (b) time histories of the vertical gap between the trailing edge of the leading foil and the leading edge of the trailing foil, and (c) the relationship between mean stable distance and maximum vertical gap in different cases. Instantaneous pressure coefficient contours of tandem foils at $t/T = 0.2$ for the cases of (d) $\phi = 1.6\pi$ and (e) $\phi = 0.1\pi$ in the fast mode.

dimensionless vertical coordinates of the trailing edge of the leading foil and the leading edge of the trailing foil.

Figure 14(a) shows the maximum value of D_V, i.e., $D_{V\max}$, in one cycle in different cases. It is clear that the fast mode is only observed in the cases with small $D_{V\max}$ (<0.46, below the blue dash-dot line). Moreover, the evolution of D_V in one cycle is illustrated in Fig. 14(b). It can be seen that the different vortex interactions are determined by the moment when $D_{V\max}$ occurs. When $D_{V\max}$ appears in the upstroke, the merging interaction happens. When $D_{V\max}$ appears in the downstroke, the broken interaction happens.

In addition, the averaged separation distance between two foils is related to the different fluid-structure interactions in the fast mode. Figure 14(c) shows the relationship between the mean separation distance ($\bar{G}/c$) and the maximum vertical gap ($D_{V\max}$) in merging and broken interactions. It is clear that in the merging interaction, $\bar{G}/c$ increases with the rise of $D_{V\max}$. However, in the broken interaction, the opposite trend can be observed. The different trends of

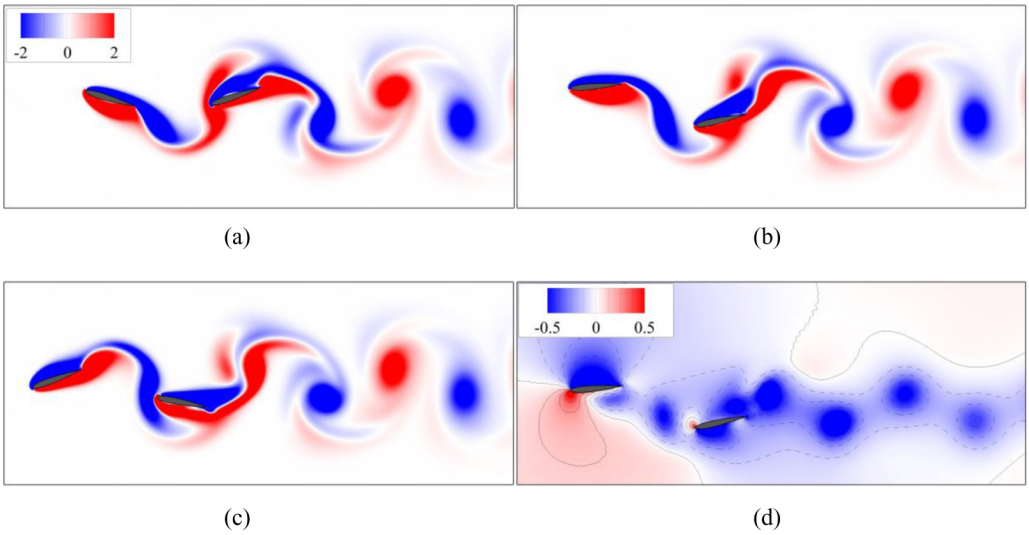

FIG. 15. Instantaneous vorticity at (a) $t = 0.1T$, (b) $0.3T$, and (c) $0.5T$ for the case of $\phi = 0.7\pi$ and $G_0 = c$. (d) Instantaneous pressure coefficient contours at $t = 0.3T$.

variation of $\bar{G}/c$ versus $D_{V\max}$ in merging and broken interactions can be qualitatively explained as follows. In the merging interaction, the TEV of the leading foil is often located near the leading edge of the trailing foil, and it induces a negative pressure region between the two foils, which is marked as the green dashed region in Fig. 14(d). Such negative pressure region has a suction effect on the trailing foil. As $D_{V\max}$ increases, the suction effect becomes weak; thus, $\bar{G}/c$ increases. In the broken interaction, the TEV of the leading foil often sheds into the wake together with the LEV of the trailing foil, which induces a positive pressure region between two foils [the green dashed region in Fig. 14(e)]. Such positive pressure region has a repulsion effect on the trailing foil. As the $D_{V\max}$ decreases, the repulsion effect becomes strong, and $\bar{G}/c$ increases.

C. Performance of slow mode

In the slow mode, only one vortex interaction is observed, i.e., the vortex locking. As shown in Figs. 15(a)–15(c), for example, the follower swims through the vortex cores. In this mode, the leader swims like the isolated one.

As shown in Fig. 16, both the thrust and power coefficients of the leader are similar to those of the isolated foil. However, although the follower achieves the same averaged velocity of the leader, the velocity fluctuation of the follower is larger than that of the leader. This is because the thrust fluctuation of the follower is larger than that of the leader, as shown in Fig. 16(a). A possible reason is that the follower needs more thrust to balance the additional drag that is produced by the jet flow of the leader. Moreover, the follower exhibits significant energy extraction during $t = 0.3T - 0.4T$ and $0.4T$–$0.9T$ in one cycle, as shown in Fig. 16(b). The reason is that the vortex-induced velocity can produce positive pressure at the leading edge of the follower when it is close to a vortex, which results in the lift with the same direction of the flapping motion, as shown in Figs. 15(b) and 15(d). This mode is similar to the observations in the previous work [30,31,33], and it can be qualitatively explained by the hydrodynamic mechanism in which the thrust is determined by the effective flapping speed [31,33]. For example, as shown in Fig. 15(a), the follower propels at the equilibrium position. If the follower propels ahead of the equilibrium position, the direction of the vortex-induced velocity is the same as that of the flapping direction, which would reduce its effective flapping speed. Thus, the follower would generate low thrust and move backward to the

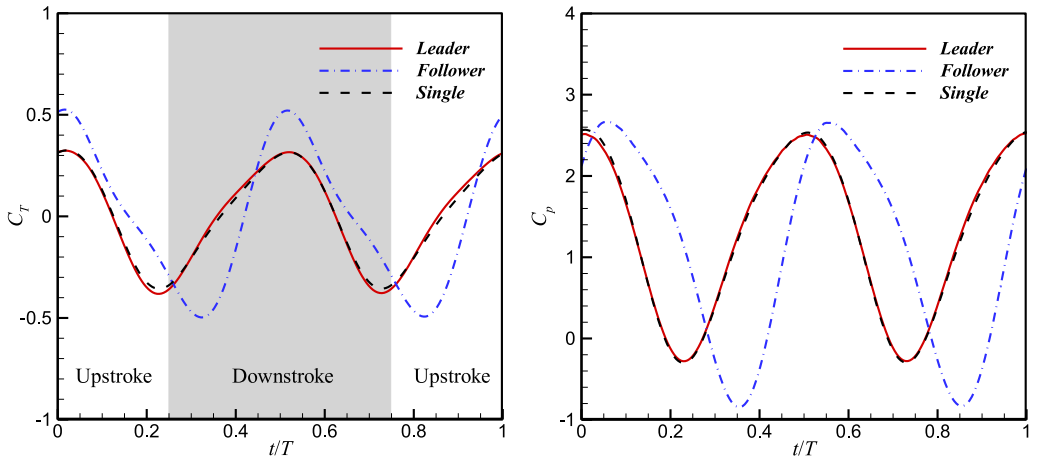

FIG. 16. The time histories of (a) thrust coefficients and (b) power coefficients of tandem foils ($\phi = 0.7\pi$ and $G_0 = c$) and a single foil.

equilibrium position. Similarly, if the follower propels behind the equilibrium position, the vortex-induced velocity has the opposite direction as compared with the flapping motion, which would increase its effective flapping speed. Consequently, the follower would generate large thrust and move forward to the equilibrium position.

Figure 17 is the side elevation of Fig. 5(a) without the cases in the fast mode, which is viewed along the G_0/c direction. It is clear that for a fixed initial spacing, the stable separation distance in the slow mode is linearly affected by the phase difference, but there is a discontinuity point which is determined by G_0. The slope of linear variation is approximately –0.41, which is close to the value of $-L/(2\pi)$, where L is the propulsive length in one period of an isolated flapping foil with the same parameters. Consequently, the relationship between the stable distance and the phase difference can be described as

$$\bar{G} \approx -\frac{L}{2\pi}\phi + C, \tag{11}$$

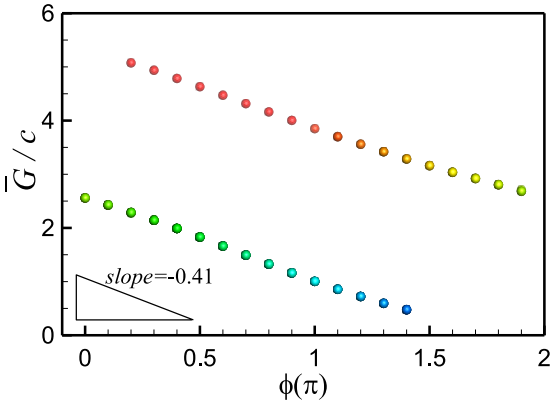

FIG. 17. The side elevation of Fig. 5(a) viewed along the G_0/c direction.

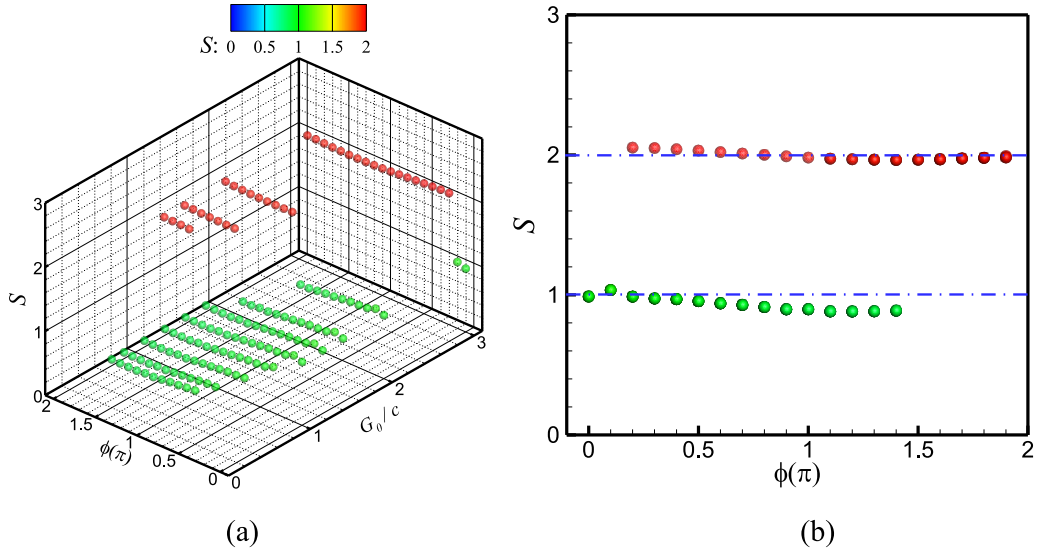

FIG. 18. (a) The quantized result of the stable distance between two foils in the slow mode; (b) is the planform of (a).

where C is a constant which represents the discontinuity point. Inspired by the work reported in the literature [33], C can be defined as $C \approx NL$, where N is integer value such as $N = 1, 2 \cdots$. Thus, the stable gap of two tandem foils in arbitrary phase difference can be quantized as

$$S = \frac{\bar{G}}{L} + \frac{\phi}{2\pi} \approx N. \tag{12}$$

When $\phi = 0$, i.e., the in-phase motion appears, the quantized equation is similar to that proposed by Ramananarivo and coauthors [33]. The quantized result is illustrated in Fig. 18. It is clear that the values of S are close to the integer values. Namely, the stable distance can be quantized with phase difference in the slow mode, as formulated by Eq. (12). Ramananarivo *et al.* [33] indicated that the stable gap between two in-phase heaving foils is integer multiples of the propulsive length of the leader in one period. Considering the phase difference between tandem foils, the integer S here indicates that in the slow mode, the asynchronous follower propels along the same trajectory as that of the in-phase follower, but ahead of the in-phase one with a distance which can be approximated as $g \approx \frac{\phi}{2\pi} L$.

IV. CONCLUSIONS

The collective locomotion of two tandem flapping foils with phase difference is numerically studied in the current work, in which both foils, respectively, are driven by the harmonic motions. The two-dimensional viscous flow over the flapping foils is simulated by an immersed boundary-simplified circular function–based gas kinetic method. A wide range of phase difference ϕ is selected for study, i.e., 0.0π–1.9π with an interval of 0.1π. The achieved results indicate that the collective locomotion is greatly affected by the phase difference. Two distinct collective modes are classified according to the variation of the propulsive velocity, i.e., the fast mode and slow mode.

In the fast mode, both foils achieve high velocity and propulsive efficiency as compared with the single foil, and the stable distance is small (approximately $0.1c$–$0.3c$). The fast mode is only observed in part of the range of phase difference, i.e., $\phi = 0.0\pi - 0.1\pi$ and $1.5\pi - 1.9\pi$, with appropriate initial distance. Meanwhile, it is found that the fast mode is related to the maximum

vertical distance between the trailing edge of the leader and the leading edge of the follower. In addition, two distinct vortex interactions are observed in the fast mode, i.e., merging interaction and broken interaction. In the merging interaction, the leading edge vortex of the leader is captured by the follower, which results in the weak trailing edge vortex of the leader but a strong trailing edge vortex of the follower. In the broken interaction, the leading edge vortex of the follower sheds into the wake together with the trailing edge vortex of the leader, and induces the trailing edge vortex of the follower to be broken into two parts. Which kind of interaction occurs depends on the phase difference.

In the slow mode, both foils produce the same averaged velocity which is close to that of the isolated foil. In the range of $\phi = 0.3\pi - 1.4\pi$, the slow mode is the unique collective mode observed in the current work. In the rest of the range of ϕ, the slow mode only occurs when the initial distance is large enough. In addition, the stable distance between two foils in the slow mode can be quantized with phase difference. Moreover, it should be pointed out that the follower also has hydrodynamic benefit in both fast and slow modes, but the leader can only achieve hydrodynamic benefit in the fast mode. Furthermore, the leader achieves the highest efficiency and velocity in the fast mode when $\phi = 0.1\pi$, but the follower obtains the highest efficiency in the fast mode when $\phi = 1.6\pi$. The results obtained in the current work may shed some light on understanding the collective behavior of fish schools and bird flocks.

ACKNOWLEDGMENTS

J.W. acknowledges the support of the National Natural Science Foundation of China (Grant No. 11622219), the Research Fund of State Key Laboratory of Mechanics and Control of Mechanical Structures (Nanjing University of Aeronautics and Astronautics) (Grant No. MCMS-0117G01), and the Fundamental Research Funds for the Central Universities (Grant No. NE2017102). X.L. acknowledges the support of the Funding for Outstanding Doctoral Dissertation in NUAA (Grant No. BCXJ19-02). This work is also supported by the Priority Academic Program Development of Jiangsu Higher Education Institutions (PAPD).

[1] J. Krebs, Fish schooling, Nature **264**, 701 (1976).
[2] C. K. Hemelrijk and H. Hildenbrandt, Schools of fish and flocks of birds: Their shape and internal structure by self-organization, Interface Focus **2**, 726 (2012).
[3] R. W. Whittlesey, S. Liska, and J. O. Dabiri, Fish schooling as a basis for vertical axis wind turbine farm design, Bioinspiration Biomimetics **5**, 035005 (2010).
[4] K. Streitlien, G. S. Triantafyllou, and M. S. Triantafyllou, Efficient foil propulsion through vortex control, AIAA J. **34**, 2315 (1996).
[5] D. H. Cushing and F. R. H. Jones, Why do fish school, Nature **218**, 918 (1968).
[6] J. C. Liao, A review of fish swimming mechanics and behaviour in altered flows, Philos. Trans. R. Soc., B **362**, 1973 (2007).
[7] I. Ashraf, R. Godoy-Diana, J. Halloy, B. Collignon, and B. Thiria, Synchronization and collective swimming patterns in fish (Hemigrammus bleheri), J. R. Soc., Interface **13**, 20160734 (2016).
[8] I. Ashraf, H. Bradshaw, T. T. Ha, J. Halloy, R. Godoy-Diana, and B. Thiria, Simple phalanx pattern leads to energy saving in cohesive fish schooling, Proc. Natl. Acad. Sci. USA **114**, 9599 (2017).
[9] S. J. Portugal, T. Y. Hubel, J. Fritz, S. Heese, D. Trobe, B. Voelkl, S. Hailes, A. M. Wilson, and J. R. Usherwood, Upwash exploitation and downwash avoidance by flap phasing in ibis formation flight, Nature **505**, 3992014.
[10] H. Weimerskirch, J. Martin, Y. Clerquin, P. Alexandre, and S. Jiraskova, Energy saving in flight formation, Nature **413**, 697 (2001).

[11] D. Weihs, Hydromechanics of fish schooling, Nature **241**, 290 (1973).
[12] J. C. Liao, D. N. Beal, G. V. Lauder, and M. S. Triantafyllou, Fish exploiting vortices decrease muscle activity, Science **302**, 1566 (2003).
[13] S. Marras, S. S. Killen, J. Lindstrom, D. J. McKenzie, J. F. Steffensen, and P. Domenici, Fish swimming in schools save energy regardless of their spatial position, Behav. Ecol. Sociobiol. **69**, 219 (2015).
[14] M. Lighthill, *Mathematical Biofluiddynamics* (Society for Industrial and Applied Mathematics, Philadelphia, 1975).
[15] B. L. Partridge and T. J. Pitcher, Evidence against a hydrodynamic function for fish schools, Nature **279**, 418 (1979).
[16] J. R. Usherwood, M. Stavrou, J. C. Lowe, K. Roskilly, and A. M. Wilson, Flying in a flock comes at a cost in pigeons, Nature **474**, 494 (2011).
[17] J. Deng, X.-M. Shao, and Z.-S. Yu, Hydrodynamic studies on two traveling wavy foils in tandem arrangement, Phys. Fluids **19**, 113104 (2007).
[18] P. A. Dewey, D. B. Quinn, B. M. Boschitsch, and A. J. Smits, Propulsive performance of unsteady tandem hydrofoils in a side-by-side configuration, Phys. Fluids **26**, 041903 (2014).
[19] S.-Y. Chen, Y.-H. J. Fei, Y.-C. Chen, K.-J. Chi, and J.-T. Yang, The swimming patterns and energy-saving mechanism revealed from three fish in a school, Ocean Eng. **122**, 22 (2016).
[20] C. K. Hemelrijk, D. A. P. Reid, H. Hildenbrandt, and J. T. Padding, The increased efficiency of fish swimming in a school, Fish Fish. **16**, 511 (2015).
[21] V. Raspa, R. Godoy-Diana, and B. Thiria, Topology-induced effect in biomimetic propulsive wakes, J. Fluid Mech. **729**, 377 (2013).
[22] B. M. Boschitsch, P. A. Dewey, and A. J. Smits, Propulsive performance of unsteady tandem hydrofoils in an in-line configuration, Phys. Fluids **26**, 0519012014.
[23] A. P. Maertens, A. Gao, and M. S. Triantafyllou, Optimal undulatory swimming for a single fish-like body and for a pair of interacting swimmers, J. Fluid Mech. **813**, 301 (2017).
[24] M. S. U. Khalid, I. Akhtar, and H. Dong, Hydrodynamics of a tandem fish school with asynchronous undulation of individuals, J. Fluids Struct. **66**, 19 (2016).
[25] A. Gao and M. S. Triantafyllou, Independent caudal fin actuation enables high energy extraction and control in two-dimensional fish-like group swimming, J. Fluid Mech. **850**, 304 (2018).
[26] G. D. Xu, W. Y. Duan, and W. H. Xu, The propulsion of two flapping foils with tandem configuration and vortex interactions, Phys. Fluids **29**, 097102 (2017).
[27] L. E. Muscutt, G. D. Weymouth, and B. Ganapathisubramani, Performance augmentation mechanism of in-line tandem flapping foils, J. Fluid Mech. **827**, 484 (2017).
[28] N. Vandenberghe, J. Zhang, and S. Childress, Symmetry breaking leads to forward flapping flight, J. Fluid Mech. **506**, 147 (2004).
[29] X. Zhang, S. Ni, S. Wang, and G. He, Effects of geometric shape on the hydrodynamics of a self-propelled flapping foil, Phys. Fluids **21**, 103302 (2009).
[30] X. Zhu, G. He, and X. Zhang, Flow-Mediated Interactions Between Two Self-Propelled Flapping Filaments in Tandem Configuration, Phys. Rev. Lett. **113**, 238105 (2014).
[31] Z.-R. Peng, H. Huang, and X.-Y. Lu, Hydrodynamic schooling of multiple self-propelled flapping plates, J. Fluid Mech. **853**, 587 (2018).
[32] A. D. Becker, H. Masoud, J. W. Newbolt, M. Shelley, and L. Ristroph, Hydrodynamic schooling of flapping swimmers, Nat. Commun. **6**, 8514 (2015).
[33] S. Ramananarivo, F. Fang, A. Oza, J. Zhang, and L. Ristroph, Flow interactions lead to orderly formations of flapping wings in forward flight, Phys. Rev. Fluids **1**, 071201 (2016).
[34] L. M. Yang, C. Shu, W. M. Yang, Y. Wang, and J. Wu, An immersed boundary-simplified sphere function-based gas kinetic scheme for simulation of 3D incompressible flows, Phys. Fluids **29**, 083605 (2017).
[35] X. Lin, S. Guo, J. Wu, and J. Nan, Aerodynamic performance of a flapping foil with asymmetric heaving motion near a wall, J. Bionic Eng. **15**, 636 (2018).
[36] E. Akoz and K. W. Moored, Unsteady propulsion by an intermittent swimming gait, J. Fluid Mech. **834**, 149 (2017).

[37] J. Wu and C. Shu, Implicit velocity correction-based immersed boundary-lattice Boltzmann method and its applications, J. Comput. Phys. **228**, 1963 (2009).

[38] Z. J. Wang, Unsteady forces and flows in low Reynolds number hovering flight: two-dimensional computations vs robotic wing experiments, J. Exp. Biol. **207**, 449 (2004).

[39] N. Arora, A. Gupta, S. Sanghi, H. Aono, and W. Shyy, Flow patterns and efficiency power characteristics of a self-propelled heaving rigid flat plate, J. Fluid Struct. **66**, 517 (2016).